

Atlas of CMFGEN Models for OB Massive Stars

C. R. FIERRO,^{1,2} J. BORISSOVA,^{2,3} J. ZSARGÓ,¹ A. DÍAZ-AZUARA,⁴ R. KURTEV,^{2,3} L. GEORGIEV,^{4,5}
S. RAMÍREZ ALEGRIÁ,^{2,3} AND F. PEÑALOZA²

Received 2014 September 01; accepted 2015 March 23; published 2015 April 20

ABSTRACT. We present an atlas of 173 synthetic spectra of stars, with mass from 9 to $120 M_{\odot}$, covering the region of the OB main sequence stars in the H–R diagram. The spectra were calculated with the stellar atmosphere code CMFGEN, assuming solar metallicity in the ZAMS. In order to study the effect of rotation on the chemical composition of the stellar atmosphere, we calculated two sets of models: with metallicity changed by rotation when the star evolves and maintaining solar metallicity throughout the same evolutionary track. For each model, we calculated its synthetic spectra in the UV (900–2000 Å), optical (3500–7000 Å), and near IR (10,000–30,000 Å). We show the utility of this atlas, obtaining preliminary models for three stars in the field of the VVVCL086 cluster, comparing their IR observed spectra with the ones of the atlas. This process was done in a few hours, while the standard procedure to obtain such models could take several weeks.

1. INTRODUCTION

Stellar atmosphere models are a useful tool to understand the physical parameters and the chemical composition of the stars. Nowadays, there are several stellar atmosphere codes, some of which are able to compute the atomic populations assuming nonlocal thermodynamic equilibrium (NLTE) and incorporating the effects of the line-blanketing, e.g., TLUSTY (Hubeny & Lanz 1995), FASTWIND (Santolaya-Rey et al. 1997; Puls et al. 2005), and CMFGEN (Hillier & Miller 1998).

There are several methods to find a model that successfully reproduces the observed spectrum of a star. It is possible to calculate a grid of models, covering a range of values for the main stellar parameters, e.g., an effective temperature–log gravity (T_{eff} – $\log g$) grid. The codes able to calculate a model in a short time are the best suited for working under this philosophy; the main disadvantage is the simplification of the physical processes involved, e.g., plane-parallel atmosphere in TLUSTY.

The codes which incorporate the largest number of physical processes consume more computational resources but they produce more realistic models, e.g., CMFGEN. In this case, the standard procedure is to fix some parameters while fitting the others, then changing the fixed parameters while fitting new

ones, and so on, iterating until the solution for all parameters is stable. Under this philosophy the computational time consumed to get a model for a particular object may become a severe limitation. When analyzing a large sample of objects this becomes a serious disadvantage.

With the aim of obtaining realistic models and reducing the computation time, we have developed an atlas of synthetic spectra calculated with the CMFGEN code, covering the region of the OB main sequence stars with mass from 9 to $120 M_{\odot}$ in the H–R diagram. These synthetic spectra can be used as the starting point in the calculation of the models for several objects. In § 2, we describe the atmosphere models included in this atlas, the assumptions made to calculate them, and the parameters derived from these. In § 3, we describe the atlas, the parameter space, and the covered region within the diagram H–R. In order to show the utility of the atlas, we present an application example in § 4, comparing the IR observed spectra of three stars in the field of the VVVCL086 cluster with the models in the atlas we obtained the stellar parameters, the age, and the metallicity of the cluster. Finally, in § 5, we present our conclusions.

2. ATMOSPHERE MODELS

The stellar atmosphere models were calculated with the CMFGEN code (Hillier & Miller 1998). This code computes the continuum and line formation in non-LTE, solving the radiative transfer and statistical equilibrium equations in spherical geometry. A hydrostatic structure can be computed below the sonic point. This allows the simultaneous treatment of spectral lines formed in the atmosphere, the stellar wind, and in the transition region between both. Such features make it particularly well suited to the study of massive OB stars with winds.

The elements included in the calculation of the models were H, He, C, N, O, Si, P, S, and Fe. For the model ions, CMFGEN

¹ Departamento de Física, Escuela Superior de Física y Matemáticas, Instituto Politécnico Nacional, México, D.F., México; cfierro@dfa.uv.cl, jzsargo@esfm.ipn.mx.

² Instituto de Física y Astronomía, Facultad de Ciencias, Universidad de Valparaíso, Av. Gran Bretaña 1111, Playa Ancha, Casilla 5030, Valparaíso, Chile; jura.borissova@uv.cl, radostin.kurtev@uv.cl, sebastian.ramirez@uv.cl, francisco.penaloza@uv.cl.

³ Millennium Institute of Astrophysics, MAS, Santiago, Chile.

⁴ Instituto de Astronomía, Universidad Nacional Autónoma de México, México, Apartado Postal 70-264; alf@astro.unam.mx.

⁵ Deceased.

TABLE 1
SUPER LEVELS/LEVELS FOR THE DIFFERENT IONIZATION STAGES INCLUDED IN THE MODELS

Element	I	II	III	IV	V	VI	VII	VIII	IX	X	XI	XII
H	20/30	1/1
He	27/39	13/30	1/1
C	...	40/92	10/10	14/14	1/1
N	...	52/84	26/26	34/60	45/67	1/1
O	...	54/123	25/45	53/72	75/152	13/13	1/1
Si	20/34	22/33	52/203	66/279	1/1
P	36/178	16/62	1/1
S	13/28	51/142	31/98	28/58	1/1
Fe	19/182	10/80	14/153	53/324	52/490	70/808	72/1155	1/1

utilizes the concept of “super levels,” by which levels of similar energies are grouped together and treated as a single level in the statistical equilibrium equations (Hillier & Miller 1998). The stellar models include 27–29 explicit ions of the different elements as function of their T_{eff} . Table 1 summarizes the levels and super levels included in the models. The atomic data references are given in Herald & Bianchi (2004).

3. THE ATLAS

The Atlas includes synthetic spectra in the UV, optical, and near IR, generated from the 176 atmosphere models calculated with CMFGEN, covering the region of the OB main sequence stars with mass from 9 to $120 M_{\odot}$.

In order to constrain appropriately the parameters of the models, we use the evolutionary tracks of Ekström et al. (2012) corresponding to solar metallicity ($Z = 0.014$) at the zero age of the main sequence (ZAMS). For any trace, each point corresponds to a star with specific values of T_{eff} , luminosity (L), and stellar mass (M). We calculated several models along each track with steps of 2500 K in T_{eff} , while the stellar radius and $\log g$ were calculated to get the L and M corresponding to the track.

With the purpose of observing the effect of abundance in the spectral lines, we calculate two sets of models based on the evolutionary tracks with rotation and without it. Due to the mixing induced by rotation, the chemical composition of the stellar photosphere changes when star evolves (Maeder et al. 2004). In the models with rotation the He and N abundances increase when the star evolves from the ZAMS to the end of MS while the C and O abundances decrease. On the other hand, in the models without rotation, the abundances remain unchanged from the ZAMS to advanced stages of the star (Ekström et al. 2012). Figure 1 shows the location of the models and the evolutionary tracks in the H–R diagram.

The elements included in the calculation of all models were H, He, C, N, O, Si, P, S, and Fe. The values of H, He, C, N, and O were taken from the tables of Ekström et al. (2012). For consistency, we assumed the solar metallicity reported by Asplund et al. (2009) for the Si, P, S, and Fe in all models.

The early OB stars may have winds. To model the stellar wind, CMFGEN requires values for the mass loss rate (\dot{M}), terminal velocity (v_{inf}), and the *clumping factor* of the wind (cf). This increases the complexity of the grid. In order to make an appropriate comparison between models without getting lost in the parameter space, we fixed average values for the wind

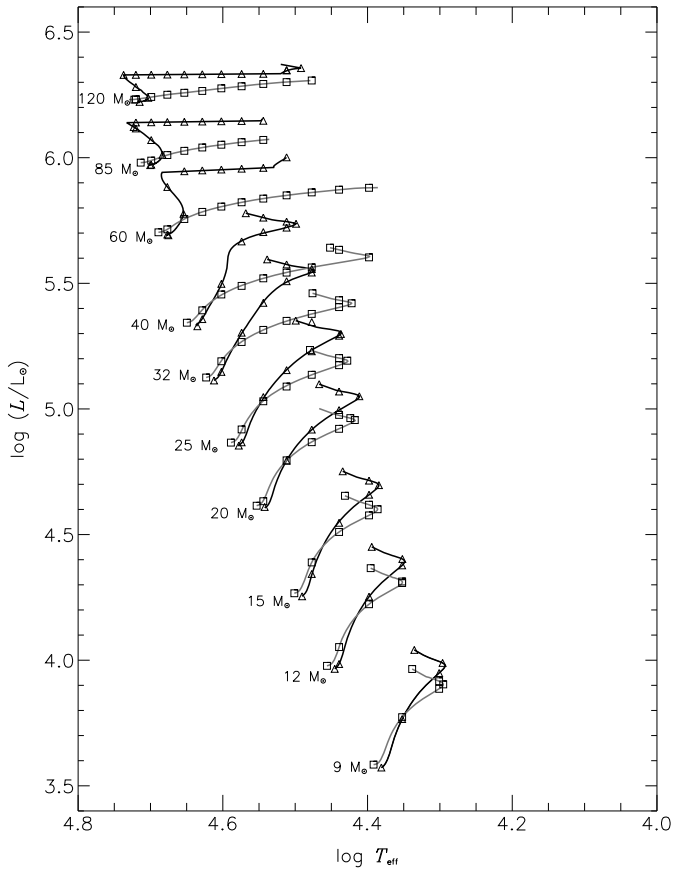


FIG. 1.—Position of the models in the H–R diagram and the evolutionary tracks of Ekström et al. (2012). Triangles and squares represent models with and without rotation, respectively.

parameters. All models included in the atlas were calculated with the same terminal velocity, $v_{\text{inf}} = 1000 \text{ km s}^{-1}$. The mass loss rate varies from 1×10^{-9} for the models with $M_{\text{ZAMS}} = 9 M_{\odot}$ to 5×10^{-6} for the models with $M_{\text{ZAMS}} = 120 M_{\odot}$; however, the value of \dot{M} is the same for all the models over the same evolutionary track with and without rotation. All models were calculated assuming a homogeneous wind ($cf = 1.0$).

In the evolutionary tracks of Ekström, the models with rotation have an equatorial rotation velocity $v_{\text{rot}} = 0.4 v_{\text{crit}}$, where v_{crit} is the critical velocity, defined as

$$v_{\text{crit}} = \sqrt{\frac{GM}{R_{\text{eq}}}} = \sqrt{\frac{2GM}{3R_{\text{pol}}}}, \quad (1)$$

where R_{eq} and R_{pol} are the equatorial and polar radii of the star that deviate from a sphere due to rotation. For consistency with the evolutionary tracks, the theoretical rotation velocities of the models of this atlas are 0.4 times the v_{crit} reported by Ekström et al. (2012). Thereby, the rotation velocities range from 161 km s^{-1} for the model of $9 M_{\odot}$ at the end of the main

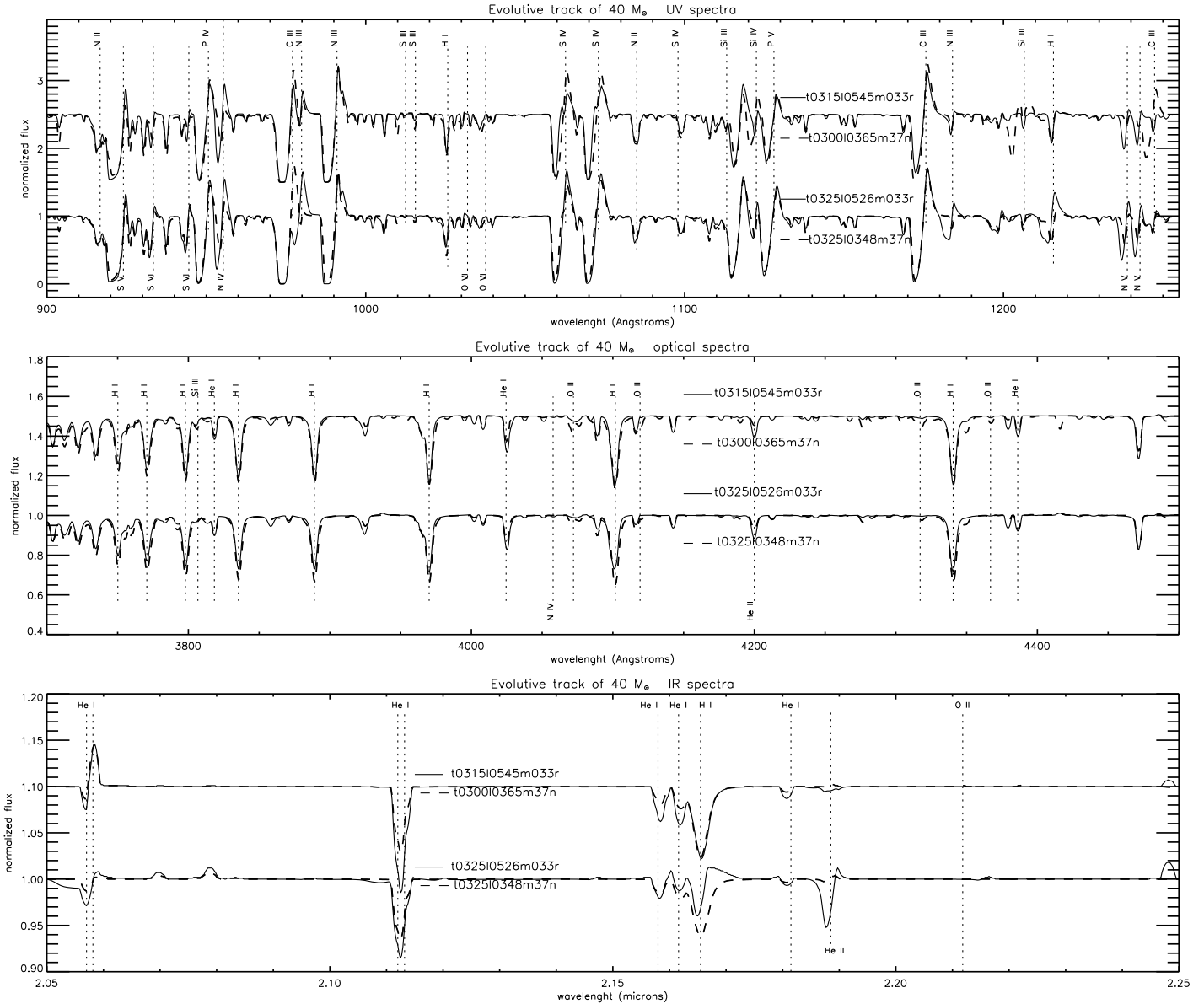


FIG. 2.—A sample of the spectra in the atlas. We plotted four models on the evolutive track of $40 M_{\odot}$. Solid lines show models with rotation and dashed lines show models without rotation. These plots show only part of the UV, optical, and near IR spectra; data files covering the wavelength range of $900\text{--}2000 \text{ \AA}$, $3500\text{--}7000 \text{ \AA}$, and $10,000\text{--}30,000 \text{ \AA}$ are available on websites and electronic version of this article.

TABLE 2

WAVELENGTH IDENTIFICATION FOR THE SPECTRAL LINES MARKED IN FIG. 2

UV spectrum					
$\lambda(A^\circ)$	Ion	$\lambda(A^\circ)$	Ion	$\lambda(A^\circ)$	Ion
916.70	N II	1015.57	S III	1122.50	Si IV
924.00	S V	1025.72	H I	1175.66	C III
933.38	S VI	1031.91	O VI	1184.02	N III
944.52	S VI	1037.61	O VI	1206.50	Si III
950.66	P IV	1062.66	S IV	1211.01	P V
955.33	N IV	1072.97	S IV	1215.67	H I
977.02	C III	1085.00	N II	1238.83	N V
979.87	N III	1098.93	S IV	1242.82	N V
990.98	N III	1110.01	P V	1247.38	C III
1012.50	S III	1113.20	Si III		
Optical spectrum					
$\lambda(A^\circ)$	Ion	$\lambda(A^\circ)$	Ion	$\lambda(A^\circ)$	Ion
3750.15	H I	3889.05	H I	4119.22	O II
3770.63	H I	3970.17	H I	4199.94	He II
3797.90	H I	4024.53	He I	4317.14	O II
3806.70	Si III	4057.76	N IV	4340.46	H I
3818.38	He I	4072.15	O II	4366.89	O II
3835.38	H I	4101.73	H I	4386.13	He I
IR spectrum					
λ (microns)	Ion	λ (microns)	Ion	λ (microns)	Ion
2.0570	He I	2.1132	He I	2.1885	He II
2.0581	He I	2.1580	He I	2.2118	O II
2.0700	C IV	2.1616	He I	2.2487	C II
2.0790	C IV	2.1655	H I	2.3097	He I
2.0836	C IV	2.1815	He I	2.4271	Si IV
2.1120	He I	2.1849	N II		

sequence to 396 km s^{-1} for the model of $120 M_\odot$ at the ZAMS. In order to incorporate the rotation effect into the spectral lines, the synthetic spectra calculated by the CMFGEN code were rotationally broadened using the program ROTIN3. This program is part of the TLUSTY code (Hubeny & Lanz 1995).

In order to visualize the changes in the spectral lines throughout the evolution of the star, the spectra were grouped following each evolutionary track. Figure 2 shows the UV, optical, and IR spectra for a sample of the models in the atlas. We plotted with solid lines the spectra of the models with rotation, and with dashed lines the spectra of the models without rotation. For consistency, these were rotationally broadened at the v_{rot} of the model with rotation at the same T_{eff} . Table 2 shows only the lines marked on such spectra; however, many other transitions have been considered in the models.

Tables 3 and 4 summarize the parameters of the 176 models included in the atlas. The plots of spectra UV, optical, and IR of all models are available in two websites: <https://sites.google.com/site/modelsobmassivestars/>, maintained by C. Fierro, and replicated in <http://www.astroscu.unam.mx/atlas/index.html>, maintained by IA-UNAM. The files containing wavelength in Angstroms and normalized flux can be downloaded from these websites and from the electronic version of this article. The wavelength range covered by the synthetic spectra is 900–2000 Å for UV, 3500–7000 Å for visual, and 10,000–30,000 Å for near IR.

By comparing the spectra of the models with similar T_{eff} and progenitor in the ZAMS, with and without rotation, it may be noted that the less massive and evolved stars show similar spectral lines. In contrast, the most massive and evolved stars show significant differences in their spectral lines when rotation is considered.

TABLE 3
MODELS WITH ROTATION

Model	T_{eff} (K)	L/L_\odot	$\log g$	M/M_\odot	$\dot{M}(M_\odot \text{ yr}^{-1})$	$v_{\text{rot}}(\text{km s}^{-1})$	He/H	C/H^a	N/H^a	O/H^a
$9 M_\odot$ track										
t0240l0003m009r	24,000	3740	4.300	9	1×10^{-9}	232	0.092	2.67	0.65	4.98
t0225l0005m009r	22,500	5831	3.990	9	1×10^{-9}	194	0.093	2.46	0.91	4.94
t0200l0008m009r	20,000	8890	3.602	9	1×10^{-9}	156	0.095	1.85	1.78	4.74
t0216l0010m009r	21,600	10,989	3.647	9	1×10^{-9}	161	0.096	1.73	1.97	4.69
$12 M_\odot$ track										
t0278l0092m012r	27,900	9239	4.288	12	1×10^{-8}	248	0.092	2.67	0.65	4.98
t0250l0017m012r	25,000	17,895	3.810	12	1×10^{-8}	188	0.094	2.02	1.52	4.80
t0225l0023m012r	22,500	23,840	3.475	12	1×10^{-8}	158	0.098	1.62	2.20	4.61
t0248l0028m012r	24,800	28,259	3.595	12	1×10^{-8}	167	0.099	1.55	2.34	4.58
$15 M_\odot$ track										
t0309l0017m015r	30,900	17,960	4.276	15	5×10^{-8}	260	0.092	2.67	0.65	4.98
t0300l0022m015r	30,000	22,040	4.139	15	5×10^{-8}	239	0.092	2.65	0.68	4.97
t0275l0035m015r	27,500	35,220	3.775	15	5×10^{-8}	195	0.095	1.96	1.67	4.73
t0250l0045m015r	25,000	45,830	3.495	15	5×10^{-8}	165	0.100	1.58	2.40	4.52
t0242l0049m015r	24,200	49,740	3.403	15	5×10^{-8}	157	0.103	1.49	2.62	4.43
t0250l0051m015r	25,000	51,840	3.440	15	5×10^{-8}	159	0.104	1.46	2.69	4.43
t0272l0056m015r	27,200	56,480	3.554	15	5×10^{-8}	170	0.104	1.46	2.69	4.43

TABLE 3 (Continued)

Model	T_{eff} (K)	L/L_{\odot}	$\log g$	M/M_{\odot}	$\dot{M}(M_{\odot} \text{ yr}^{-1})$	$v_{\text{rot}}(\text{km s}^{-1})$	He/H	C/H^{a}	N/H^{a}	O/H^{a}
20 M_{\odot} track										
t0348l0040m020r	34,850	40,720	4.260	20	5×10^{-8}	276	0.092	2.67	0.65	4.98
t0325l0062m020r	32,500	62,190	3.945	20	5×10^{-8}	232	0.093	2.32	1.15	4.85
t0300l0082m020r	30,000	82,770	3.670	20	5×10^{-8}	196	0.097	1.88	1.97	4.58
t0275l0098m020r	27,500	98,940	3.446	20	5×10^{-8}	172	0.103	1.67	2.48	4.40
t0258l0112m020r	25,800	112,300	3.277	20	5×10^{-8}	156	0.108	1.55	2.85	4.29
t0250l0117m020r	25,000	117,300	3.206	20	5×10^{-8}	164	0.109	1.54	2.91	4.27
t0275l0118m020r	27,500	118,000	3.369	20	5×10^{-8}	166	0.109	1.54	2.91	4.27
t0293l0125m020r	29,300	125,400	3.463	20	5×10^{-8}	172	0.109	1.54	2.91	4.27
25 M_{\odot} track										
t0378l0071m025r	37,800	71,470	4.250	25	5×10^{-8}	292	0.092	2.67	0.65	4.98
t0375l0073m025r	37,500	73,640	4.219	25	5×10^{-8}	284	0.092	2.67	0.65	4.98
t0350l0111m025r	35,000	111,500	3.920	25	5×10^{-8}	236	0.094	2.31	1.26	4.78
t0325l0142m024r	32,500	142,700	3.670	24	5×10^{-8}	206	0.101	1.94	2.18	4.40
t0300l0169m024r	30,000	169,600	3.450	24	5×10^{-8}	184	0.113	1.73	2.92	4.14
t0275l0195m024r	27,500	195,600	3.233	24	5×10^{-8}	160	0.127	1.59	3.58	3.96
t0273l0198m024r	27,300	198,800	3.216	24	5×10^{-8}	156	0.128	1.58	3.66	3.49
t0300l0221m024r	30,000	221,700	3.335	24	5×10^{-8}	174	0.132	1.56	3.81	3.90
t0316l0224m024r	31,600	224,600	3.413	24	5×10^{-8}	176	0.132	1.56	3.81	3.90
32 M_{\odot} track										
t0409l0129m032r	40,944	129,800	4.236	32	1×10^{-7}	308	0.092	2.67	0.65	4.98
t0400l0140m032r	40,000	140,400	4.160	32	1×10^{-7}	292	0.092	2.67	0.65	4.98
t0375l0201m030r	37,500	201,200	3.875	30	1×10^{-7}	245	0.097	2.21	1.69	4.52
t0350l0237m030r	35,000	237,900	3.670	30	1×10^{-7}	208	0.127	1.72	3.69	3.72
t0325l0322m029r	32,500	322,300	3.391	29	1×10^{-7}	180	0.181	1.46	5.78	3.22
t0300l0349m028r	30,000	349,000	3.212	28	1×10^{-7}	164	0.198	1.42	6.30	3.14
t0300l0360m028r	30,000	360,000	3.196	28	1×10^{-7}	160	0.202	1.41	6.42	3.12
t0325l0375m028r	32,500	375,900	3.320	28	1×10^{-7}	170	0.202	1.41	6.44	3.12
t0346l0354m028r	34,600	354,400	3.470	28	1×10^{-7}	180	0.202	1.41	6.44	3.12
40 M_{\odot} track										
t0431l0213m040r	43,172	213,300	4.206	40	1×10^{-6}	320	0.092	2.67	0.65	4.98
t0425l0227m040r	42,500	227,800	4.148	40	1×10^{-6}	307	0.092	2.67	0.65	4.98
t0400l0314m038r	40,000	314,700	3.880	38	1×10^{-6}	256	0.103	2.03	2.37	4.15
t0375l0464m034r	37,500	464,200	3.553	34	1×10^{-6}	207	0.249	1.14	8.57	2.37
t0350l0505m033r	35,000	505,700	3.428	33	1×10^{-6}	184	0.285	1.09	9.64	2.25
t0325l0526m033r	32,500	526,800	3.231	33	1×10^{-6}	170	0.299	1.07	10.00	2.21
t0315l0545m033r	31,536	545,700	3.155	33	1×10^{-6}	164	0.312	1.06	10.40	2.18
t0325l0556m033r	32,500	556,500	3.205	33	1×10^{-6}	168	0.320	1.05	10.60	2.16
t0350l0577m033r	35,000	577,500	3.320	33	1×10^{-6}	176	0.320	1.05	10.60	2.16
t0370l0601m033r	37,000	601,100	3.400	33	1×10^{-6}	184	0.320	1.05	10.60	2.16
60 M_{\odot} track										
t0473l0491m060r	47,350	491,200	4.180	60	1×10^{-6}	348	0.092	2.67	0.65	4.98
t0475l0494m060r	47,500	494,700	4.183	60	1×10^{-6}	347	0.092	2.67	0.65	4.98
t0451l0598m056r	45,100	598,100	3.984	56	1×10^{-6}	304	0.102	1.88	2.73	3.92
t0475l0764m050r	47,500	764,900	3.917	50	1×10^{-6}	347	0.253	0.62	10.30	1.27
t0450l0883m045r	45,000	883,200	3.712	45	1×10^{-6}	264	0.506	0.44	17.20	0.69
t0425l0890m045r	42,500	890,200	3.606	45	1×10^{-6}	264	0.526	0.44	17.70	0.68
t0400l0897m045r	40,000	897,200	3.499	45	1×10^{-6}	264	0.547	0.45	18.20	0.66
t0375l0904m045r	37,500	904,100	3.382	45	1×10^{-6}	264	0.567	0.45	18.70	0.66
t0350l0911m044r	35,000	911,100	3.258	44	1×10^{-6}	264	0.588	0.45	19.20	0.64
t0325l1003m039r	32,500	952,800	3.034	39	1×10^{-6}	227	1.147	0.60	32.70	0.61
t0350l1021m039r	35,000	1,021,000	3.155	39	1×10^{-6}	229	1.157	0.60	32.90	0.61
t0375l1039m039r	37,500	1,039,000	3.270	39	1×10^{-6}	229	1.173	0.61	33.30	0.61
t0400l1058m039r	40,000	1,058,000	3.367	39	1×10^{-6}	230	1.189	0.61	33.70	0.61
t0425l1077m039r	42,500	1,077,000	3.464	39	1×10^{-6}	231	1.205	0.61	34.10	0.61
t0450l0985m039r	45,000	985,500	3.600	39	1×10^{-6}	231	1.222	0.62	34.40	0.62
t0473l1000m039r	47,300	1,000,000	3.690	39	1×10^{-6}	232	1.237	0.63	34.80	0.65

TABLE 3 (Continued)

Model	T_{eff} (K)	L/L_{\odot}	$\log g$	M/M_{\odot}	$\dot{M}(M_{\odot} \text{ yr}^{-1})$	$v_{\text{rot}}(\text{km s}^{-1})$	He/H	C/H^a	N/H^a	O/H^a
85 M_{\odot} track										
t0501l0934m085r	50,150	934,000	4.154	85	1×10^{-6}	372	0.092	2.67	0.65	4.98
t0500l0937m085r	50,000	937,900	4.145	85	1×10^{-6}	369	0.092	2.67	0.65	4.98
t0482l1026m076r	48,250	1,026,000	4.021	80	1×10^{-6}	336	0.100	1.73	0.30	3.79
t0500l1175m068r	50,000	1,175,000	3.986	76	1×10^{-6}	322	0.193	0.46	9.29	9.99
t0525l1307m067r	52,500	1,307,000	3.988	68	1×10^{-6}	316	0.368	0.26	14.40	0.34
t0528l1324m064r	52,850	1,324,000	3.990	67	1×10^{-6}	312	0.399	0.26	15.20	0.31
t0525l1380m064r	52,500	1,380,000	3.942	64	1×10^{-6}	312	0.542	0.23	18.60	0.27
t0500l1383m064r	50,000	1,383,000	3.855	64	1×10^{-6}	312	0.552	0.30	18.90	0.27
t0475l1387m064r	47,500	1,387,000	3.764	64	1×10^{-6}	312	0.563	0.31	19.10	0.27
t0450l1390m064r	45,000	1,390,000	3.668	64	1×10^{-6}	312	0.574	0.31	19.40	0.27
t0425l1393m064r	42,500	1,393,000	3.567	64	1×10^{-6}	312	0.595	0.31	19.70	0.27
t0400l1396m064r	40,000	1,396,000	3.459	64	1×10^{-6}	312	0.595	0.31	19.90	0.27
t0375l1399m064r	37,500	1,399,000	3.348	64	1×10^{-6}	312	0.606	0.33	20.20	0.27
t0350l1428m063r	35,000	1,428,000	3.215	63	1×10^{-6}	312	0.617	0.33	20.40	0.27
120 M_{\odot} track										
t0518l1667m120r	51,850	1,667,000	4.110	120	5×10^{-6}	396	0.092	0.27	0.654	0.498
t0505l1731m115r	50,500	1,731,000	4.030	115	5×10^{-6}	372	0.146	0.16	29.4	0.387
t0525l1911m105r	52,500	1,911,000	4.013	105	5×10^{-6}	356	0.199	2.04	10.3	0.348
t0546l2134m089r	54,600	2,134,000	3.961	89	5×10^{-6}	332	0.527	2.92	18.3	0.217
t0525l2137m088r	52,500	2,137,000	3.891	88	5×10^{-6}	332	0.534	2.95	18.5	0.219
t0500l2140m088r	50,000	2,140,000	3.805	88	5×10^{-6}	332	0.542	2.98	18.7	0.221
t0475l2142m088r	47,500	2,142,000	3.715	88	5×10^{-6}	330	0.550	0.30	18.9	0.223
t0450l2145m088r	45,000	2,145,000	3.619	88	5×10^{-6}	330	0.558	0.30	19.1	0.225
t0425l2148m088r	42,500	2,148,000	3.517	88	5×10^{-6}	330	0.566	0.31	19.3	0.226
t0400l2151m087r	40,000	2,151,000	3.412	87	5×10^{-6}	330	0.574	0.31	19.4	0.228
t0375l2154m087r	37,500	2,154,000	3.297	87	5×10^{-6}	328	0.582	0.31	19.6	0.230
t0350l2157m087r	35,000	2,157,000	3.183	87	5×10^{-6}	328	0.590	0.32	19.8	0.232
t0325l2224m080r	32,500	2,224,000	3.000	80	5×10^{-6}	272	0.904	0.45	27.2	0.308

^a $\times 10^{-4}$.

4. APPLICATION EXAMPLE: VVVCL 086

The VVV CL086 cluster (Borissova et al. 2011) is a massive cluster found in the direction of the Perseus arm ($l = 340.001$, $b = 0.293$). The observed spectra were obtained

with the ISAAC spectroscope attached at the Very Large Telescope at ESO Paranal Observatory, Chile. The observation and data reduction are described in Ramírez Alegría et al. (2014).

TABLE 4
MODELS WITHOUT ROTATION

Model	T_{eff} (K)	L/L_{\odot}	$\log g$	M/M_{\odot}	$\dot{M}(M_{\odot} \text{ yr}^{-1})$	$v_{\text{rot}}(\text{km s}^{-1})$	He/H	C/H^a	N/H^b	O/H^b
9 M_{\odot} track										
t0240l0003m009n	24,650	3840	4.327	9	1×10^{-9}	232	0.092	2.67	6.54	4.98
t0225l0005m009n	22,500	5932	3.983	9	1×10^{-9}	194	0.092	2.67	6.54	4.98
t0200l0007m009n	20,000	7692	3.665	9	1×10^{-9}	156	0.092	2.67	6.54	4.98
t0218l0009m009n	21,800	9224	3.735	9	1×10^{-9}	161	0.092	2.67	6.54	4.98
12 M_{\odot} track										
t0275l0011m012n	27,500	11,270	4.180	12	1×10^{-8}	248	0.092	2.67	6.54	4.98
t0250l0016m012n	25,000	16,700	3.840	12	1×10^{-8}	188	0.092	2.67	6.54	4.98
t0225l0020m012n	22,500	20,280	3.574	12	1×10^{-8}	158	0.092	2.67	6.54	4.98
t0248l0024m012n	24,850	23,240	3.689	12	1×10^{-8}	167	0.092	2.67	6.54	4.98
15 M_{\odot} track										
t0317l0018m015n	31,700	18,460	4.308	15	1×10^{-8}	260	0.092	2.67	6.54	4.98
t0300l0024m015n	30,000	24,300	4.090	15	1×10^{-8}	239	0.092	2.67	6.54	4.98
t0275l0032m015n	27,500	32,370	3.815	15	1×10^{-8}	195	0.092	2.67	6.54	4.98
t0250l0037m015n	25,000	37,700	3.580	15	1×10^{-8}	165	0.092	2.67	6.54	4.98
t0243l0039m015n	24,300	39,880	3.500	15	1×10^{-8}	157	0.092	2.67	6.54	4.98
t0250l0041m015n	25,000	41,560	3.538	15	1×10^{-8}	159	0.092	2.67	6.54	4.98
t0270l0045m015n	26,990	45,120	3.635	15	1×10^{-8}	170	0.092	2.67	6.54	4.98

TABLE 4 (Continued)

Model	T_{eff} (K)	L/L_{\odot}	$\log g$	M/M_{\odot}	$\dot{M}(M_{\odot} \text{ yr}^{-1})$	$v_{\text{rot}}(\text{km s}^{-1})$	He/H	C/H^a	N/H^b	O/H^a
20 M_{\odot} track										
t0357l0041m020n	35,750	41,190	4.300	20	1×10^{-8}	276	0.092	0.267	65.4	0.497
t0350l0042m020n	35,000	42,920	4.237	20	1×10^{-8}	276	0.092	0.267	65.4	0.497
t0325l0062m020n	32,500	62,430	3.943	20	1×10^{-8}	232	0.092	0.267	65.4	0.497
t0300l0073m020n	30,000	73,730	3.730	20	1×10^{-8}	196	0.092	0.267	65.3	0.497
t0275l0083m020n	27,500	83,340	3.250	20	1×10^{-8}	172	0.092	0.267	65.3	0.497
t0261l0090m020n	26,550	91,930	3.420	20	1×10^{-8}	156	0.902	0.267	65.3	0.497
25 M_{\odot} track										
t0388l0073m025n	38,800	73,450	4.280	25	1×10^{-8}	292	0.092	2.67	6.54	4.98
t0375l0082m025n	37,500	82,870	4.166	25	1×10^{-8}	284	0.092	2.67	6.54	4.98
t0350l0107m025n	35,000	107,200	3.930	25	1×10^{-8}	236	0.092	2.67	6.54	4.98
t0325l0122m024n	32,500	122,700	3.740	24	1×10^{-8}	206	0.092	0.267	65.3	0.498
t0300l0123m024n	30,000	123,000	3.597	24	1×10^{-8}	184	0.092	0.267	65.3	0.497
t0275l0149m024n	27,500	149,300	3.361	24	1×10^{-8}	160	0.092	0.267	65.3	0.497
t0267l0155m024n	26,791	155,500	3.300	24	1×10^{-8}	156	0.092	0.267	65.3	0.497
t0275l0159m024n	27,500	159,400	3.340	24	1×10^{-8}	160	0.092	0.267	65.3	0.497
t0302l0160m024n	30,200	160,000	3.500	24	1×10^{-8}	174	0.092	0.267	65.3	0.497
32 M_{\odot} track										
t0419l0133m032n	41,981	133,300	4.261	32	1×10^{-7}	308	0.092	2.67	6.54	4.98
t0400l0154m032n	40,000	154,800	4.112	32	1×10^{-7}	292	0.092	2.67	6.54	4.98
t0375l0184m031n	37,500	184,600	3.915	31	1×10^{-7}	245	0.092	2.67	6.54	4.98
t0350l0206m031n	35,000	206,300	3.743	31	1×10^{-7}	208	0.092	2.67	6.54	4.98
t0325l0224m031n	32,500	224,100	3.581	31	1×10^{-7}	180	0.092	2.67	6.54	4.98
t0300l0238m031n	30,000	238,800	3.410	31	1×10^{-7}	164	0.092	2.67	6.54	4.98
t0275l0254m030n	27,500	254,300	3.226	30	1×10^{-7}	164	0.092	2.67	6.54	4.98
t0265l0263m030n	26,500	263,300	3.170	30	1×10^{-7}	164	0.092	2.67	6.54	4.98
t0275l0270m030n	27,500	270,900	3.198	30	1×10^{-7}	164	0.092	2.67	6.54	4.98
t0300l0288m030n	30,000	288,600	3.360	30	1×10^{-7}	180	0.092	2.67	6.54	4.98
40 M_{\odot} track										
t0446l0220m040n	44,640	220,300	4.251	40	1×10^{-6}	320	0.092	2.67	6.54	4.98
t0425l0246m039n	42,500	246,800	4.110	39	1×10^{-6}	307	0.092	2.67	6.54	4.98
t0400l0285m038n	40,000	285,400	3.930	38	1×10^{-6}	256	0.092	2.67	6.54	4.98
t0375l0308m038n	37,500	308,800	3.777	38	1×10^{-6}	207	0.092	2.67	6.54	4.98
t0350l0331m037n	35,000	331,000	3.622	37	1×10^{-6}	184	0.092	2.67	6.54	4.98
t0325l0348m037n	32,500	348,800	3.467	37	1×10^{-6}	170	0.092	2.67	6.54	4.98
t0300l0365m037n	30,000	365,700	3.305	37	1×10^{-6}	164	0.092	2.67	6.54	4.98
t0275l0380m037n	27,500	380,300	3.135	37	1×10^{-6}	168	0.092	2.67	6.54	4.98
t0250l0401m037n	25,000	401,100	2.946	37	1×10^{-6}	176	0.092	2.67	6.54	4.98
t0275l0429m037n	27,500	429,800	3.135	37	1×10^{-6}	184	0.092	2.67	6.54	4.98
60 M_{\odot} track										
t0489l0504m060n	48,900	504,700	4.226	60	5×10^{-6}	348	0.092	0.264	0.654	0.498
t0475l0518m060n	47,500	518,500	4.160	60	5×10^{-6}	347	0.092	2.67	6.54	4.98
t0450l0570m058n	45,000	570,100	4.010	58	5×10^{-6}	304	0.092	2.67	6.54	4.98
t0425l0608m056n	42,500	608,500	3.870	56	5×10^{-6}	264	0.092	2.67	6.54	4.98
t0400l0638m055n	40,000	638,800	3.735	55	5×10^{-6}	264	0.092	2.67	6.54	4.98
t0375l0664m054n	37,500	664,500	3.596	54	5×10^{-6}	264	0.092	2.67	6.54	4.98
t0350l0687m053n	35,000	687,300	3.455	53	5×10^{-6}	264	0.092	2.67	6.54	4.98
t0325l0708m053n	32,500	708,100	3.310	53	5×10^{-6}	227	0.092	2.67	6.54	4.98
t0300l0772m052n	30,000	772,400	3.129	52	5×10^{-6}	227	0.092	2.67	6.54	4.98
t0275l0745m052n	27,500	745,700	3.000	52	5×10^{-6}	227	0.092	2.67	6.54	4.98
t0250l0758m051n	25,000	758,800	2.820	51	5×10^{-6}	227	0.092	2.67	6.54	4.98
85 M_{\odot} track										
t0518l0955m085n	51,850	955,600	85	4.197	1×10^{-6}	372	0.092	2.67	6.54	4.98
t0500l0973m084n	50,000	973,500	84	4.124	1×10^{-6}	369	0.092	2.67	6.54	4.98
t0475l01024m080n	47,500	1,024,400	80	3.995	1×10^{-6}	312	0.092	2.67	6.54	4.98
t0450l01064m078n	45,000	1,064,800	78	3.870	1×10^{-6}	312	0.092	2.67	6.54	4.98
t0425l01097m076n	42,500	1,097,900	76	3.745	1×10^{-6}	312	0.092	2.67	6.54	4.98
t0400l1126m074n	40,000	1,126,100	74	3.618	1×10^{-6}	312	0.092	2.67	6.54	4.98
t0375l1153m073n	37,500	1,153,600	73	3.490	1×10^{-6}	312	0.092	2.67	6.54	4.98
t0350l1176m072n	35,000	1,176,800	72	3.355	1×10^{-6}	312	0.092	2.67	6.54	4.98

TABLE 4 (Continued)

Model	T_{eff} (K)	L/L_{\odot}	$\log g$	M/M_{\odot}	$\dot{M}(M_{\odot} \text{ yr}^{-1})$	$v_{\text{rot}}(\text{km s}^{-1})$	He/H	C/H^{a}	N/H^{b}	O/H^{a}
120 M_{\odot} track										
t0528I1702m120n	52,800	1,702,000	120	4.132	5×10^{-6}	356	0.092	2.67	6.54	4.98
t0525I1707m119n	52,500	1,707,000	119	4.117	5×10^{-6}	332	0.092	2.67	6.54	4.98
t0500I1744m114n	50,000	1,744,000	114	4.005	5×10^{-6}	332	0.092	2.67	6.54	4.98
t0475I1780m110n	47,500	1,780,000	110	3.889	5×10^{-6}	330	0.092	2.67	6.54	4.98
t0450I1812m103n	45,000	1,812,000	103	3.654	5×10^{-6}	330	0.092	2.67	6.54	4.98
t0425I1843m099n	42,500	1,843,000	99	3.521	5×10^{-6}	330	0.092	2.67	6.54	4.98
t0400I1888m097n	40,000	1,888,000	97	3.390	5×10^{-6}	330	0.092	2.67	6.54	4.98
t0375I1924m096n	37,500	1,924,000	96	3.390	5×10^{-6}	328	0.092	2.67	6.54	4.98
t0350I1965m094n	35,000	1,965,000	94	3.250	5×10^{-6}	328	0.092	2.67	6.54	4.98
t0325I1999m093n	32,500	1,999,000	93	3.106	5×10^{-6}	272	0.092	2.67	6.54	4.98

^a $\times 10^{-4}$.^b $\times 10^{-5}$.

In order to find preliminary models for three stars in the field of the VVVCL086 cluster, we compare its IR observed spectra with the ones of the atlas. This process was done in a few hours, while the standard procedure to obtain a model for only one object by running several generations of models, changing only one of the parameters while the others remained fixed, consumed several weeks.

4.1. Stellar Parameters

Figure 3 shows the best fit of the observed spectra with the models of the atlas. Table 5 summarizes the physical parameters and the chemical composition obtained for each star from the models.

We can notice that Br $_{\gamma}$ line is underestimated in models for objects 2 and 3. This line may be affected by the clumping factor (Lenorzer et al. 2004). The fit could be improved by using $cf \leq 1.0$.

The effective temperatures obtained from the models are slightly larger than those indicated by the spectral types reported by Ramírez Alegría et al. (2014) for these stars. This difference

may be caused by the line-blanketing treatment in the CMFGEN models. Line-blanketing changes the atmospheric structure: due to the metallic lines, photons are more backscattered toward the inner atmosphere. The ionization is then increased in the formation region of the He lines used for the spectral classification. Consequently, when using CMFGEN models, there is a discrepancy for one or two subtypes (Martins et al. 2005; Martins & Schaefer 2003).

4.2. Cluster Stars Members

The wavelength in the observed spectra has an rms uncertainty of 0.5 pixels, which corresponds to $\sim 30 \text{ km s}^{-1}$ in radial velocity. Because of this, the radial velocity was discarded as a criterion for membership in the cluster.

Figure 4 shows the position of the objects 2, 3, and 4 in the H–R diagram, from its preliminary models. In this, we overplotted isochrones for 1, 3, and 5 Myrs, calculated from evolutionary tracks. From the isochrones, object 2 has an age close to 1 Myr, while objects 3 and 4 have between 3 and 5 Myr. We conclude that objects 3 and 4 are cluster members, while object 2 is not a cluster member. The cluster age was estimates

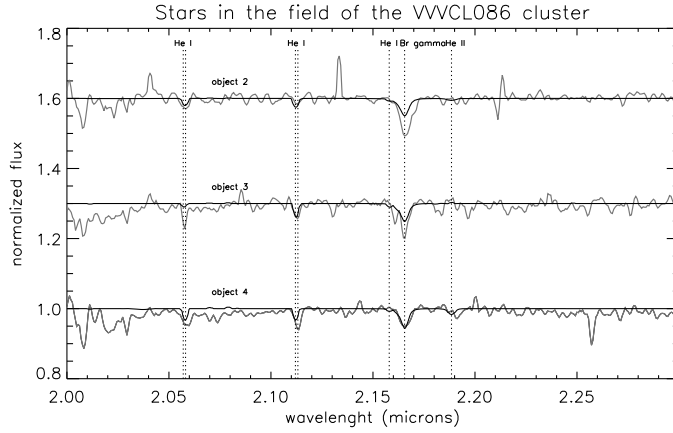


FIG. 3.—IR spectra of three stars in the field of the VVVCL086 cluster, and the best fit with the models of the atlas.

TABLE 5
STELLAR PARAMETERS

Parameter	Object_2	Object_3	Object_4
Model	t0375I0082m25n	t0350I0111m025r	t0375I0201m30r
T_{eff} (K)	37,500	35,000	37,500
L/L_{\odot}	82,870	111,500	201,200
$\log g$	4.166	3.920	3.875
M/M_{\odot}	25	25	30
He/H	0.092	0.094	0.097
$C/H \times 10^{-4}$	2.67	2.31	2.21
$N/H \times 10^{-5}$	6.54	12.60	16.90
$O/H \times 10^{-4}$	4.98	4.78	4.52
τ_{evol} (yrs)	1.53×10^6	4.39×10^6	3.73×10^6
Spectral type ^a	B2–3 V	O9–B0 V	O9 V

^a Ramírez Alegría et al. (2014).

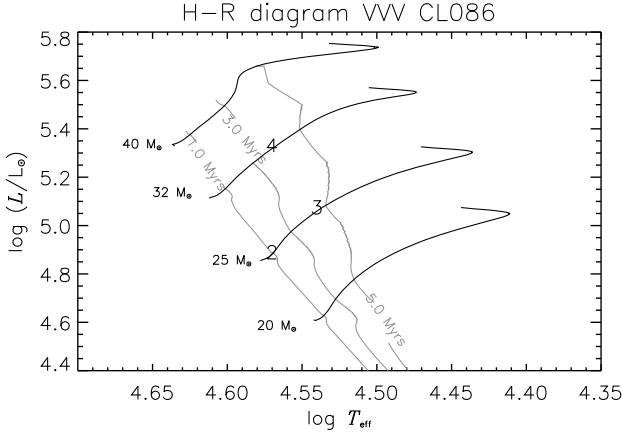


FIG. 4.—Position of Objects 2, 3, and 4 in the H-R diagram. We overplotted isochrones for 1, 3, and 5 Myrs.

in 4.0 ± 1 Myrs. These results agree with the results obtained by Ramírez Alegría et al. (2014) using the cluster photometric data. The metallicity of the cluster obtained from the models is close to that of the Sun.

5. CONCLUSIONS

We present an atlas of synthetic spectra, from 176 models calculated with the CMFGEN code. These models cover the region of H-R diagram populated by the OB main sequence stars with mass from 9 to $120 M_{\odot}$. The atlas includes the UV, visual, and IR spectra.

The models included in the atlas incorporates many of the physical processes taking place in stellar atmospheres (e.g., line-blanketing, spherical symmetry, and calculation of populations nLTE), producing realistic models. Each model includes 27–29 explicit ions of nine different elements (H, He, C, N, O, Si, P, S, and Fe) as a function of their T_{eff} . We use evolutionary tracks to constrain the values of the T_{eff} , $\log g$, and luminosity of each model. All these features allow us to produce realistic and reliable models for the analysis of a variety of objects observed.

The analysis of three stars of the cluster VVV CL086 shows the utility of this atlas to obtain a model able to reproduce acceptably the observed spectrum. This model allows us to know several parameters of the star (e.g., T_{eff} , $\log g$, L, M, and chemical composition), as well as of the cluster (metallicity and age). Usually, this analysis is time consuming. This atlas reduces the time required for such analysis.

We express our acknowledgment to the anonymous referee for his comments and suggestions, which helped us to improve this work. C. R. Fierro was supported by projects 176144 and 24754-IPN of CONACYT. J. Borissova, R. Kurtev, and S. Ramírez Alegría are supported by the Ministry of Economy, Development, and Tourisms Millennium Science Initiative through grant IC120009, awarded to The Millennium Institute of Astrophysics (MAS). J. Borissova, R. Kurtev, and S. Ramírez Alegría are supported by Fondecyt No. 1120601, No. 1130140, and No. 3140605. J. Zsargó is supported by CONACYT grant 168632 CB-2011-01.

REFERENCES

- Asplund, M., Grevesse, N., Sauval, A. J., & Scott, P. 2009, A&A Rev., 47, 481
- Borissova, J., Bonatto, C., Kurtev, R., et al. 2011, A&A, 532, A 131
- Ramírez Alegría, S., Borissova, J., Chené, A. N., et al. 2014, A&A, 564, L 9
- Ekström, S., Georgy, C., Eggenberger, P., Meynet, G., et al. 2012, A&A, 537, 146
- Herald, J. E., & Bianchi, L. 2004, ApJ, 609, 378
- Hillier, D. J., & Miller, D. 1998, ApJ, 496, 407
- Hubeny, I., & Lanz, T. 1995, ApJ, 439, 875
- Lenorzer, A., Mokiem, M. R., de Koter, A., & Puls, J. 2004, A&A, 422, 275
- Martins, F., & Schaerer, D. 2003, in ASP Conf. Ser. 288, Stellar Atmosphere Modeling, ed. I. Hubeny, D. Mihalas, & K. Werner (San Francisco: ASP)
- Martins, F., Schaerer, D., & Hiller, J. 2005, A&A, 436, 1049
- Maeder, A., Meynet, G., & Hirschi, R. 2004, EAS, 11, 77
- Puls, J., Urbaneja, M. A., Venero, R., et al. 2005, A&A, 435, 669
- Santolaya-Rey, A. E., Puls, J., & Herrero, A. 1997, A&A, 323, 488